# CHAPTER-5

## STABILITY OF MAGNETIZED COMPLEX ASTROFLUIDS WITH ATYPICAL DUST-FUGACITY EFFECTS

***Abstract:*** *In this Chapter, we investigate the dynamics of the dust acoustic wave (DAW, low-fugacity, low-frequency) and the dust Coulomb wave (DCW, high-fugacity, lower-frequency) in self-gravitating magnetized viscoelastic spherical dusty astroclouds.*[†] *It applies a generalized hydrodynamic model framework consisting of the inertial dust grains with variable charge alongside the non-thermal electrons and ions. A spherical normal mode analysis yields a unique generalized quadratic dispersion relation. It is found that the fluctuations are free from the viscoelasticity effects in the weakly coupled limit (WCL) against the strongly coupled limit (SCL). The distinctive WCL-SCL scenarios followed by low-high fugacity effects are illustratively analyzed. The results correlate consistencies with real astronomic structure formation dynamics.*

### 5.1 INTRODUCTION

It is well-known that the dust molecular clouds (DMCs) are the best sites of the interstellar medium (ISM) acting as the nurseries for stars, planets, etc. The DMCs morphologically consist of micron-sized dust grains made basically of graphite, silicate, and complex carbonaceous derivatives [1]. The massive dust grains (~0.1-10 μm) in the DMCs are susceptible to the non-local self-gravitational action collectively leading thereby to the gravitational or Jeans instability [2, 3]. It is pertinent here to note that, only the volumes of the DMCs exceeding that corresponding to the critical Jeans scale-length undergo fragmentation instability, paving the way for bounded structures to form [2, 3]. Such instabilities can also be triggered with the help of a compressive shock wave propagating naturalistically through the DMCs. It creates the initial density condensations through the mechanisms of self-gravitational (compressive) instability [4-6]. However, it is not fully clear which mechanism, gravitating dust-dust attraction or propagating shock-induced density compression, is more realistically efficient in triggering the formation dynamics of stellar structures in the DMCs.

[†]Kalita, D. and Karmakar, P. K. Adapted instabilities excited in spherical magnetized viscoelastic astroclouds with extreme dust-fugacity moderations. *European Physical Journal Plus*, 136: 479. 1-25, 2021.

In the preceding chapters, it has been highlighted that the mean dust-to-gas ratio in the DMCs differs from the canonical ISM value of 1% to 20%-30% [7, 8]. This is due to the presence of larger dust grains (~0.1-10 μm) in the clouds for which the self-gravity of the dust grains come into play [2, 3]. As a result, the abundance of dust grains varies locally due to various dust accumulative processes, such as the Jeans accretion, Bondi accretion, etc. [7, 8]. The dust grain packing in such dusty plasmas is defined by a dimensionless parameter, termed as the dust-fugacity $f = 4\pi n_{d0}\lambda_D^2 R \sim N_D(R/\lambda_D)$; where, $n_{d0}$ is the equilibrium dust number density, $\lambda_D$ is the plasma Debye length, $N_D = (4\pi/3)n_{d0}\lambda_D^3$ is the number of dust grains in the Debye sphere, and $R$ is the geometrical radius of the identical spherical grains [9-13]. It is the weighted measure of the ratio of the plasma space-charge (floating) potential to the grain surface potential contributed by the electron-ion currents (random). Based on the dust-fugacity fabric, the dusty plasmas are further classified as: (a) Tenuous (Low-fugacity, $f << 1$), (b) Dilute (Moderate-fugacity, $f \sim 1$), and (c) Dense (High-fugacity, $f >> 1$). The parameter $f$ plays as decisive factor in distinguishing the regimes for the existence of different types of dust modes, such as DAWs, DCWs, DLWs, etc. It is to be noted that the DCWs are excited purely due to the dust-charge fluctuations in the dense dusty plasmas in contrast to the DAWs and DLWs. The fugacity of such dusty plasmas interestingly varies from system to system circumstancially, such as the laboratory experiments $(f \sim 10^{-2})$, Saturnian *E*- and *G*-rings $(f \sim 10^{-4} - 10^{-3})$, Saturian *F*-ring $(f >> 10)$, Jovian ring $(f \sim 1)$, and so forth [9-13].

A good number of investigations have been done on the DCW mode dynamics by N. N Rao and his team in the past [9-13]. They have well addressed and discussed the physical mechanisms behind the DCW excitation and its dispersive features in the high-fugacity regime (HFR) of the WC dusty plasmas. In this dense plasma system with $Z_d >> 1$ and $a_d << \lambda_D$, the dust-dust Coulomb interaction dominates over the thermal pressure force. It hereby provides the restoring force (Coulombic in origin) with the inertial force (non-Coulombic in origin) sourced by the dust mass to drive the DCW modes [9, 10]. Such DCWs are excited due to the dust-charge dynamics in the ultra-low-frequency regime. In contrast, the DAWs are excited in the low-fugacity regime (LFR). The DCW excitation occurs at a frequency much lower than the DAW frequency. In the long-wavelength limit, the DCW phase speed $(C_{DC})$ is much smaller than that of the DAWs $(C_{DA})$, related as $C_{DC} = C_{DA}/\sqrt{f}$ [9, 10]. They have also investigated the effects of the non-local self-gravity

on the DCW mode excitation in the WC condition [11]. It has mainly been found that the Jeans instability occurs at much smaller critical Jeans length as compared to the DAW mode excitation [11]. The low-frequency wave damping rates, caused by the dust-charge fluctuations and the wave particle interactions, have been demonstrated to confront a good conformity between the analytical and numerical results in the LFR [12, 13]. However, the damping measures obtained analytically have been reported to go lower than the corresponding numerically obtained ones in the high-frequency HFR. Such modes are reported to exist in the SC laboratory dusty plasmas as well [13, 14]. But the theoretical studies on the DCW mode in the SC limit are yet to be made.

It is noteworthy that the previous analyses of the DCWs are based on the assumption that the electrons and ions are Maxwell-Boltzmann (MB) distributed [9-13]. But it is observed that the astrophysical and space plasmas are collisionless and WC. Their constituents have weakly coupled plasma particles contributed mostly from the velocity distributions having a high-energy tail in the non-thermal kappa-$(\kappa-)$ distribution against the conventional thermal MB-picture [15-17]. It was first proposed by Vasyliunas in describing the electron energy distribution over its full range of energy [18]. Thereafter, $\kappa-$ distribution has been widely utilized to explain numerous physical phenomena, namely the solar wind [19-22], planetary magnetospheres [23-25], outer heliosphere, and inner heliosheath [26-28], beyond the heliosphere including H $_{II}$ regions [29], and so on. Although such SC plasmas are naturalistically relevant in the astrophysical direct context of structure formation processes in hot dense astroenvirons [13], a comprehensive theoretic analysis about their diversified modal behaviours in the collective correlative perspective is yet to be formulated. It sets the focal goal to investigate the coupled dynamics of the DCWs and DAWs in the SC (viscoelastic) self-gravitating magnetized non-thermal (with $\kappa-$ distributed electrons and ions) dusty plasmas in the HFR in the GH model fabric [30, 31].

The structural overview of the content layout illuminating the concept mapping illustratively offered in this proposed work is schematically depicted in a chart-flow as follows:

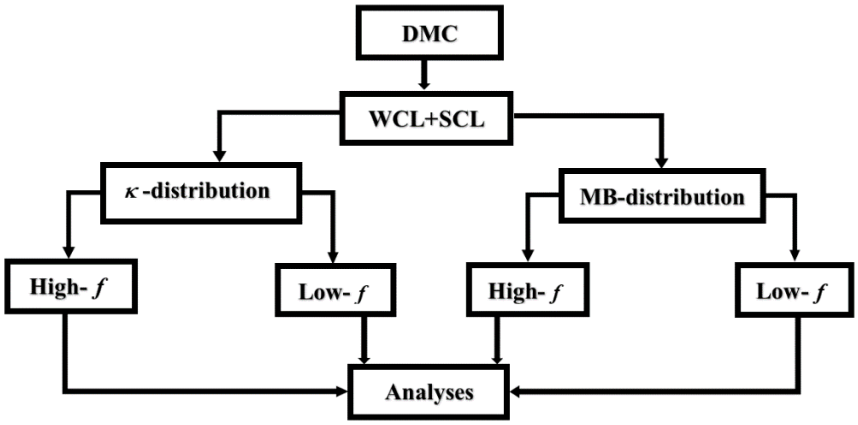


## 5.2 PHYSICAL MODEL AND FORMALISM

We consider a self-gravitating magnetized viscoelastic multi-component spherically symmetric DMC evolving on the astrophysical fluid scales of space and time. It is assumed that the interstellar magnetic field originates from convective (circulation) dynamics of the charged species. The spherically symmetric geometry enables us to reduce the 3-D problem into 1-D problem with the polar and azimuthal geometric contributions fully ignored without any loss of generality. At this backdrop, it is worth mentioning that the formation of prestellar cores via the self-gravitational instabilities are well-known to evolve usually as spherical structures in geometrical shape. As a consequence, the consideration of spherical geometry allows us to model the global cloud fragmentation and evolution into protostars in a simplified way self-consistently. It has already been reported that the magnetized Cartesian (planar) clouds [32, 33] and cylindrical (non-planar) clouds [34] are magnetically subcritical under the flux freezing condition, which is a local conservation law of the magnetic flux lines across the surface of the confined plasma fluid. Such subcritical clouds are not suitable for the gravitational collapse and protostar formation [35]. In contrast, the spherical clouds become magnetically supercritical and undergo cloud collapse even when the flux freezing condition holds, e.g., RCW 38 in the H II regions [36, 37]. It justifies our spherical geometry consideration of the magnetized DMCs. The model postulates made here can be well validated in the H II regions of the spherical DMCs sensibly. Further correlated examples are the Lagoon Nebula (M8) and Trifid Nebula (M20) in Sagittarius [1]; Rosette Nebula (NGC 244) in Monoceros [1]; etc.

The model DMC considered here comprises of the WC tiny (lighter) electrons $(e)$ and (less lighter) ions $(i)$ each having relatively high-thermal energy, and the SC micron-sized (heavier) dust particles $(d)$ having relatively low-thermal energy. The lighter non-

thermal species are thermostatistically assumed to be $\kappa-$distributed. The solid dust grains are dispersed in the gaseous ionized plasma medium treated in the GH framework in the asymptotically zero limit of the constitutive mean free path relative to the DMC dimension. The dust grains become electrically charged due to the continuous inflow (outflow) of electrons and ions flux onto (from) the grain surface. This repeated random inflow-outflow of the plasma fluxes from the dust surface causes the dust charge to fluctuate continuously. Here, the dusty plasma is a non-thermalized one as the dust grains are much colder than the electrons and the ions, i.e., $T_e$, $T_i >> T_d$ as $m_e, m_i << m_d$. Here, $m_{(j=e,i,d)}$ are the masses of the electrons, ions and dust grains, respectively. $T_{(j=e,i,d)}$ are their corresponding temperatures (in Kelvin) of the respective individual species. The constituent weightier dust grains are electrically charged via the contact electrification processes in the infinitely extended complex plasma background [29,30]. The grains actively participate in the collective dynamics and constitute a star-forming dusty plasma clouds [30]. The entire composite plasma system confined in a spherically symmetric geometry is freely assumed to form a quasi-neutral hydrostatic homogeneous equilibrium configuration at least initially on the self-gravitational spatiotemporal scales.

The basic dynamical equations here consist of the $\kappa-$distributed number densities of the electrons $(n_e)$ and ions $(n_i)$ in the dimensional form with all usual symbols [19-29], which in the coordination space $(r, t)$ in the non-relativistic regime, are given respectively as

$$n_e = n_{e0}\left[1-\frac{e\varphi}{k_B T_e\left(\kappa_e-1.5\right)}\right]^{-(\kappa_e-0.5)}, \tag{5.1}$$

$$n_i = n_{i0}\left[1+\frac{e\varphi}{k_B T_i\left(\kappa_i-1.5\right)}\right]^{-(\kappa_i-0.5)}. \tag{5.2}$$

where, $n_{e0}$ $(n_{i0})$ is the electron (ion) equilibrium number density. $\varphi$ is the electrostatic potential due to the charged density fields of the constituent fluids conjointly. As already mentioned above, our DMC model is a charge-fluctuating one at the cost of the thermal currents of the electrons and ions on the dust surfaces randomly. The loss-gain distribution dynamics of the electron-ion fluxes resulting in recombination-ionization processes on the dust surface are well tailored and monitored by $\varphi$ in equations (5.1)-(5.2). Lastly, $\kappa_{e,i}\,(>1.5)$ is the non-thermality or superthermality parameter for electrons and ions arising because of the Tsallis thermostatistics [19-29]. The dust fluid is governed by the fully

closed set of the hydrodynamic equations together with the charge dynamics equation given respectively as

$$\frac{\partial n_d}{\partial t}+\frac{1}{r^2}\frac{\partial}{\partial r}\left(r^2\, n_d\, v_{dr}\right)=0\,, \tag{5.3}$$

$$\left\{1+\tau_m\left(\frac{\partial}{\partial t}+v_{dr}\,\frac{\partial}{\partial r}\right)\right\}\left\{\left(\frac{\partial}{\partial t}+v_{dr}\,\frac{\partial}{\partial r}\right)v_{dr}+\left(\frac{\gamma_d\, k_B\, T_d}{m_d n_d}\right)\frac{\partial n_d}{\partial r}+\left(\frac{q_d}{m_d}\right)\frac{\partial \varphi}{\partial r}+\frac{\partial \psi}{\partial r}+\right.$$

$$\left.\left(\frac{B_\phi}{m_d n_d \mu_0\, r}\right)\frac{\partial}{\partial r}\left(rB_\phi\right)\right\}=\frac{1}{m_d n_d}\left(\varsigma+\frac{4}{3}\eta\right)\left\{\left(\frac{2}{r}\right)\frac{\partial v_{dr}}{\partial r}+\frac{\partial^2 v_{dr}}{\partial r^2}\right\}-\frac{2}{m_d n_d}\left(\varsigma+\frac{1}{3}\eta\right)\frac{v_{dr}}{r^2}\,, \tag{5.4}$$

$$\frac{\partial B_\phi}{\partial t}+\frac{1}{r}\frac{\partial}{\partial r}\left(r\, v_{dr}\, B_\phi\right)=0\,, \tag{5.5}$$

$$\frac{1}{r^2}\frac{\partial}{\partial r}\left(r^2\frac{\partial \varphi}{\partial r}\right)=-\frac{1}{\varepsilon_0}\left[e\left(n_i-n_e\right)+q_d n_d\right], \tag{5.6}$$

$$\frac{1}{r^2}\frac{\partial}{\partial r}\left(r^2\frac{\partial \psi}{\partial r}\right)=4\pi G\, m_d n_d\,, \tag{5.7}$$

$$\frac{\partial q_d}{\partial t}+v_{dr}\,\frac{\partial q_d}{\partial r}=I_e^{\kappa}+I_i^{\kappa}\,, \tag{5.8}$$

where, all the notations used are generic in nature [10-19]. $n_d$ is the dust population density, $v_{dr}$ is the radial velocity of the dust fluid, $q_d=-Z_d\, e$ is the instantaneous dust-charge. $\tau_m$ is the viscoelastic relaxation time. $\gamma_d$ is the specific heat ratio in adiabatic process. $\psi$ is the gravitational potential that arises due to the material density fields associated with the heavy dust grains. Then, the symbol, $B_\varphi$, designates the instantaneous magnetic field (acting azimuthally). $\eta$ and $\varsigma$ are the shear viscosity and bulk viscosity coefficients offering resistance to shear flow and to volumetric bulk expansion, respectively. We assume $\eta$ and $\varsigma$ to be constant on the Jeans fluid scales of space and time. The $\kappa-$distributed electron and ion currents, $I_e^{\kappa}$ and $I_i^{\kappa}$, flowing on the dust grain surfaces embedded in the plasma are calculated with the help of a standard probe (orbit-limited motion (OLM)) theory given with all the customary notations [38], respectively, as

$$I_e^{\kappa}=-\left\{\frac{2\sqrt{\pi\left(\kappa_e-1.5\right)}\, e\, R^2\, n_{e0}\, v_e}{\kappa_e\left(\kappa_e-1\right)}\right\}\left\{\frac{\Gamma(\kappa_e+1)}{\Gamma(\kappa_e-0.5)}\right\}\left\{1-\frac{2e}{m_e\left(\kappa_e-1.5\right)v_e^2}\left(\varphi+\frac{1}{4\pi\varepsilon_0}\frac{q_d}{R}\right)\right\}^{-\kappa_e+1}\,, \tag{5.9}$$

$$I_i^{\kappa}=-\left\{\frac{2\sqrt{\pi\left(\kappa_i-1.5\right)}\, e\, R^2\, n_{i0}\, v_i}{\kappa_i\left(\kappa_i-1\right)}\right\}\left\{\frac{\Gamma(\kappa_i+1)}{\Gamma(\kappa_i-0.5)}\right\}\left\{1+\frac{2e\varphi}{m_i\left(\kappa_i-1.5\right)v_i^2}\right\}^{-\kappa_i}$$

$$\left\{1+\frac{2e}{m_i(\kappa_i-1.5)v_i^2}\left(\varphi-\frac{1}{4\pi\varepsilon_0}\frac{q_d(\kappa_i-1)}{R}\right)\right\}, \tag{5.10}$$

where, $v_j=(2k_BT_j/m_j)^{1/2}$ is the thermal speed of the energetic j$^{th}$ species of the plasma constituent particles $(j=e,i)$; and $\Gamma(\kappa)=(n-1)!$ is the gamma function [38].

Several remarks pertinent to our model setup are in order. It may be noted that equation (5.3) contains neither a source term nor a sink term on the RHS. It is because of the fact that, on the astronomical observational scales of space and time, the global dust population density remains constant in the absence of any kind of source or sink of the dust grains. In addition, the usual diffusion processes, such as mass diffusion, thermal energy diffusion, etc. are ignored in equation (5.4), as it has no significant effect on the perturbation dynamics of the gravitational instability in the GH fabric [39]. It may be speculated that the unperturbed (equilibrium) thermodynamics of the dusty cloud is governed by an equation of adiabatic state, $P_d=K_d(\rho_d)^{\gamma_d}$, where $K_d$ is the adiabatic constant of the dust fluid. It is in contrast with the thermostatistical states of the non-thermal electrons and ions. The radial part of the differential evolution equation representing the electromagnetic inductive effects in the considered fluid in terms of the non-radial magnetic field (azimuthal $B_\varphi$) and radial velocity field (central $v_{dr}$) is given in equation (5.5). The closure property of the complex multicomponent model formalism is obtained with the help of the electrostatic Poisson equation (equation (5.6)) and the gravitational Poisson equation (equation (5.7)). It means that the charge and mass density fields respectively produce the long-range electrostatic and gravitational potentials in a coupled form.

The constituent heavier dust microspheres are constantly bombarded with the random non-thermal currents of the lighter electrons and less lighter ions. It, hereby, renders the grains electrically charged in a statistically fluctuating manner. This dust-charging process is electrodynamically depicted with the help of an appropriately closed form of the electric charge conservation law (equation (5.8)). The effect of the magnetic field on the dust-charging dynamics is neglected as and when the size of the dust grains is much smaller than the electron-ion Larmor radii [40, 41]. The temperature throughout the cloud is approximated not to vary on the astrophysical spatiotemporal fluid scales we are interested in. We ignore the uncertainty or fluctuation in the temperature likely to be caused by the Doppler broadening (due to the MB-distribution), Lorentz broadening (due to collisional effects), and so forth [42].

The aim of the current investigation is to explore the evolutionary dynamics of the linear stability of the spherically symmetric DMC in the GH fabric relative to the centre of the entire cloud mass distribution. As a result, the relevant physical parameters $(F)$ characterizing the DMC evolution undergo small-scale (linear) perturbation $(F_1)$ around their hydrostatic homogenous equilibrium values $(F_0)$ such that the approximation of weak fluctuations, $F_1 << F_0$, is well validated. It is further assumed that the perturbed variables grow homologously as concentric spherical waves with a common eigen frequency $(\omega)$ and wavenumber $(k)$ along merely the radial direction [8, 43] as

$$F(r,t) = F_0 + F_1\left(\frac{1}{r}\right)\exp\left[-i(\omega t - kr)\right]; \tag{5.11}$$

$$F = \left[n_e \;\; n_i \;\; n_d \;\; v_{dr} \;\; q_d \;\; \varphi \;\; \psi \;\; B_\varphi\right]^T, \tag{5.12}$$

$$F = \left[n_{e0} \;\; n_{i0} \;\; n_{d0} \;\; 0 \;\; q_{d0} \;\; 0 \;\; 0 \;\; B_{\varphi 0}\right]^T, \tag{5.13}$$

$$F = \left[n_{e1} \;\; n_{i1} \;\; n_{d1} \;\; v_{dr1} \;\; q_{d1} \;\; \varphi_1 \;\; \psi_1 \;\; B_{\varphi 1}\right]^T. \tag{5.14}$$

The above mathematical technique transforms the fluctuation dynamics from the coordination space $(r,t)$ into the wave space $(k,\omega)$. As a result, the spatiotemporal linear operators in the spherical geometry get autotransformed as $\partial/\partial r \to (ik - r^{-1})$, $\partial/\partial t \to (-i\omega)$ and $\partial^2/\partial r^2 \to [(-k^2 + 2r^{-2}) - i(2kr^{-1})]$. Application of equations (5.11)-(5.14) in equations (5.1)-(5.10) gives the respective perturbed forms of the physical variables cast as

$$n_{e1} = +n_{e0}\left(\alpha^e \frac{e\varphi_1}{k_B T_e}\right), \tag{5.15}$$

$$n_{i1} = -n_{i0}\left(\alpha^i \frac{e\varphi_1}{k_B T_i}\right), \tag{5.16}$$

where, $\alpha^j = \dfrac{\kappa_j - 0.5}{\kappa_j - 1.5}$, $(j = e,i)$ (5.17)

$$n_{d1} = \left\{\frac{1}{i\omega}\left(\frac{1}{r} + ik\right)n_{d0}\right\}v_{dr1}, \tag{5.18}$$

$$(1 - i\omega\tau_m)\left[-i\omega v_{dr1} + \left(ik - \frac{1}{r}\right)\left\{\left(\frac{\gamma_d v_{td}^2}{2n_{d0}}\right)n_{d1} + \left(\frac{q_{d0}}{m_d}\right)\varphi_1 + \psi_1\right\} + ik\left(\frac{B_{\varphi 0}}{m_d n_{d0}\mu_0}\right)B_{\varphi 1}\right]$$

$$= -\frac{1}{m_d n_{d0}}\left\{k^2\chi + \frac{2}{r^2}\left(\varsigma + \frac{\eta}{3}\right)\right\}, \tag{5.19}$$

where, $v_{td} = \sqrt{2k_B T_d / m_d}$ is the dust thermal speed and $\chi = \varsigma + (4/3)\eta$ is the effective generalized viscosity associated with the dust fluid.

$$B_{\varphi 1} = B_{\varphi 0}\left(\frac{k}{\omega} v_{dr1}\right), \tag{5.20}$$

$$\varphi_1 = \frac{1}{\varepsilon_0 k^2}\left[e\left(n_{i1} - n_{e1}\right) + q_{d0} n_{d1} + n_{d0} q_{d1}\right], \tag{5.21}$$

$$\psi_1 = -4\pi G m_d\left(\frac{n_{d1}}{k^2}\right), \tag{5.22}$$

$$-i\omega q_{d1} = I_{e1}^{\kappa} + I_{i1}^{\kappa}\ ; \tag{5.23}$$

where, the perturbed currents $I_{e1}^{\kappa}$ and $I_{i1}^{\kappa}$ associated with the non-thermal electrons and ions are respectively given as

$$I_{e1}^{\kappa} = -\left\{\frac{4\sqrt{\pi}\, e^2 R^2 n_{e0}}{\kappa_e\sqrt{(\kappa_e - 1.5)}\, m_e v_e}\right\}\left\{\frac{\Gamma(\kappa_e + 1)}{\Gamma(\kappa_e - 0.5)}\right\}\left\{1 - \frac{1}{4\pi\varepsilon_0}\frac{2e q_{d0}}{m_e R(\kappa_e - 1.5) v_e^2}\right\}^{-\kappa_e}\left(\varphi_1 + \frac{1}{4\pi\varepsilon_0}\frac{q_{d1}}{R}\right), \tag{5.24}$$

$$I_{i1}^{\kappa} = -\left\{\frac{4\sqrt{\pi}\, e^2 R^2 n_{i0}}{\kappa_i\sqrt{(\kappa_i - 1.5)}\, m_i v_i}\right\}\left\{\frac{\Gamma(\kappa_i + 1)}{\Gamma(\kappa_i - 0.5)}\right\}\left[\left\{1 - \frac{1}{4\pi\varepsilon_0}\frac{2e q_{d0}\kappa_i}{m_i R(\kappa_i - 1.5) v_i^2}\right\}\varphi_1 + \frac{1}{4\pi\varepsilon_0}\frac{q_{d1}}{R}\right]. \tag{5.25}$$

Using equations (5.24)-(5.25) in equation (5.23), one obtains

$$q_{d1} = -4\pi\varepsilon_0 R\left(\frac{\Omega_{c2}^{\kappa}}{\Omega_{c1}^{\kappa} - i\omega}\right)\varphi_1, \tag{5.26}$$

where, $\Omega_{c1}^{\kappa}$ and $\Omega_{c2}^{\kappa}$ are the dust-charging frequencies contributed by the homologous fluctuations in the dust charge and in the electric potential [9-13] given respectively as

$$\Omega_{c1}^{\kappa} = \frac{4\sqrt{\pi}\, e^2 R}{4\pi\varepsilon_0}\left[\left\{\frac{n_{i0}}{\kappa_i\sqrt{(\kappa_i - 1.5)}\, m_i v_i}\right\}\left\{\frac{\Gamma(\kappa_i + 1)}{\Gamma(\kappa_i - 0.5)}\right\}\right.$$

$$\left. + \left\{\frac{n_{e0}}{\kappa_e\sqrt{(\kappa_e - 1.5)}\, m_e v_e}\right\}\left\{\frac{\Gamma(\kappa_e + 1)}{\Gamma(\kappa_e - 0.5)}\right\}\left\{1 - \frac{1}{4\pi\varepsilon_0}\frac{2e q_{d0}}{m_e R(\kappa_e - 1.5) v_e^2}\right\}^{-\kappa_e}\right], \tag{5.27}$$

$$\Omega_{c2}^{\kappa} = \Omega_{c1}^{\kappa} - \frac{4\sqrt{\pi}\, e^2 R}{4\pi\varepsilon_0}\left[\left\{\frac{n_{i0}}{\kappa_i\sqrt{(\kappa_i - 1.5)}\, m_i v_i}\right\}\left\{\frac{\Gamma(\kappa_i + 1)}{\Gamma(\kappa_i - 0.5)}\right\}\left\{\frac{1}{4\pi\varepsilon_0}\frac{2e q_{d0}}{m_i R(\kappa_i - 1.5) v_i^2}\right\}\right., \tag{5.28}$$

Applying a method of decoupling over equations (5.15)-(5.28) followed by elimination and simplification, one gets a generalized linear dispersion relation for the collective instability

excitable in the considered viscoelastic magnetized dusty plasma given in a generic form as

$$\omega^2+\frac{i\omega}{m_d n_{d0}(1-i\omega\tau_m)}\left\{k^2\chi+\left(\frac{2}{r^2}\right)\left(\varsigma+\frac{1}{3}\eta\right)\right\}-k^2v_{dA}^2-$$

$$\left(k^2+\frac{1}{r^2}\right)\left(\frac{C_{DA}^2}{[1+k^2\lambda_{D\kappa}^2+f\Delta]}+\frac{\gamma_d v_{td}^2}{2}-\frac{\omega_{Jd}^2}{k^2}\right)=0\,; \tag{5.29}$$

where, $C_{DA}=\omega_{pd}\,\lambda_{D\kappa}$, $\omega_{pd}=(q_{d0}^2\,n_{d0}/\varepsilon_0 m_d)^{1/2}$ is the dust-plasma oscillation frequency and $\lambda_{D\kappa}=[\varepsilon_0 k_B/e^2\{(n_{e0}\alpha^e/T_e)+(n_{i0}\alpha^i/T_i)\}^{-1}]^{1/2}$ is the effective plasma Debye length modified by the $\kappa-$distributed electrons and ions. The Jeans angular frequency is $\omega_{Jd}=(4\pi G m_d n_{d0})^{1/2}$ and the Alfven wave phase velocity is $v_{dA}=B_{\varphi 0}/(\mu_0 m_d n_{d0})^{1/2}$. Besides, $\Delta=\Omega_{c2}^{\kappa}/(\Omega_{c1}^{\kappa}-i\omega)$ is the ratio of the modified dust-charging frequencies in the presence of the non-thermality effects induced by the diversified gradient factors of self-gravitational origin.

We apply the realistic approximation, $\omega<<\Omega_{c1}^{\kappa}$, which is specially needed for the DCWs to evolve in a complex plasma system [9-13]. In such circumstances, the dust grains get sufficient time to attain the equilibrium charge. It enables us to neglect the wave damping caused due to the dust-charge fluctuations [9-13]. It may be noted parallelly that in the counter regime of the perturbation frequency, $\omega>>\Omega_{c1}^{\kappa}$, the grain charge remains practically constant over one wave period [9-13]. It allows thereby only the DAWs to evolve. As a consequence, when $\omega<<\Omega_{c1}^{\kappa}$, we see that $\Delta\to\delta=\Omega_{c2}^{\kappa}/\Omega_{c1}^{\kappa}$ (i.e., $T_e,T_i>>1$ ), which reduces equation (5.29) for our focal aim to see the DCW excitation in an analytic simple form as

$$\omega^2+\frac{i\omega}{m_d n_{d0}(1-i\omega\tau_m)}\left\{k^2\chi+\left(\frac{2}{r^2}\right)\left(\varsigma+\frac{1}{3}\eta\right)\right\}-k^2v_{dA}^2-$$

$$\left(k^2+\frac{1}{r^2}\right)\left(\frac{C_{DA}^2}{[1+k^2\lambda_{D\kappa}^2+f\delta]}+\frac{\gamma_d v_{td}^2}{2}-\frac{\omega_{Jd}^2}{k^2}\right)=0\,. \tag{5.30}$$

Clearly, equation (5.30) is the generalized linear dispersion relation depicting the considered fluctuations excitable in the magnetized viscoelastic spherically symmetric DMC in the low-frequency regime ($\omega<<\Omega_{c1}^{\kappa}$) for a wide $f-$range. We are interested in the full dispersive and propagatory features of the fluctuation dynamics (governed by equation (5.30)) in the extreme $f-$regimes. Therefore, equation (5.30) is subject to two

distinct limiting instability categories, hydrodynamic regime (WC) and kinetic regime (SC), both in the LFR and HFR as follows.

a) Hydrodynamic limit:

In the WCL, $\omega\tau_m << 1$ [30, 31], equation (5.30) reduces to

$$\omega^2 = \left(k^2 + \frac{1}{r^2}\right)\left[\frac{C_{DA}^2}{(1+k^2\lambda_{D\kappa}^2 + f\delta)} + \frac{\gamma_d v_{td}^2}{2} - \frac{\omega_{Jd}^2}{k^2}\right] + k^2 v_{dA}^2 . \tag{5.31}$$

In the LFR, $f\delta << 1$ [9-13], the dust-charge fluctuations ($q_{d1}$) can be neglected as mentioned before. The restoring force needed for the wave propagation is provided by the electrostatic plasma potential fluctuations caused by the electron-ion charge density field perturbations (via $n_{e1}$ and $n_{i1}$). It leads to the DAW excitation given by the reduced form of equation (5.31) as

$$\omega^2 = \left(k^2 + \frac{1}{r^2}\right)\left[\frac{C_{DA}^2}{(1+k^2\lambda_{D\kappa}^2)} + \frac{\gamma_d v_{td}^2}{2} - \frac{\omega_{Jd}^2}{k^2}\right] + k^2 v_{dA}^2 . \tag{5.32}$$

In the cold unmagnetized plasma in the plane geometry approximation, equation (5.32) can be simplified to yield the phase velocity and group velocity of the DAW in the LFR as $(v_{DA})_p = C_{DA}(1+k^2\lambda_{D\kappa}^2)^{-1/2}$ and $(v_{DA})_g = (v_{DA})_p(1+3k^2\lambda_{D\kappa}^2)(1+k^2\lambda_{D\kappa}^2)^{-1}$, respectively. In the long-wavelength limit, the corresponding quantities are $(v_{DA})_p = C_{DA}$ and $(v_{DA})_g = (v_{DA})_p$. In addition, in the short-wavelength limit, the quantities get respectively transformed as $(v_{DA})_p = (k\lambda_{D\kappa})^{-1} C_{DA}$ and $(v_{DA})_g = 3(v_{DA})_p$. Thus, it may be herewith inferred that the LFR mode (DAW) is dispersive in the short-wavelength regime and non-dispersive in the long-wavelength regime with the minimum existential scale-length, $\lambda_{D\kappa}$.

In the HFR, $f\delta >> 1$ [9-13], with $Z_d >> 1$, the cumulative $q_{d1}$ results in the grain-surface potential fluctuations via $\psi_{d1} \sim q_{d1}/R$. At low-frequency, the charge quasi-neutrality condition renders the plasma potential to go on the same order as the grain surface potential (i.e., $|\varphi_1| \sim |\psi_{d1}|$). Since in the HFR, $a_d << \lambda_{D\kappa}$, the Coulomb interaction among the grains due to the surface potential is dominated. It provides the restoring force needed for the DCW propagation in this HFR describable with the reduced form of equation (5.31) as

$$\omega^2 = \left(k^2 + \frac{1}{r^2}\right)\left[\frac{C_{DC}^2}{\delta}\left(1 + \frac{k^2}{4\pi n_{d0} R\delta}\right)^{-1} + \frac{\gamma_d v_{td}^2}{2} - \frac{\omega_{Jd}^2}{k^2}\right] + k^2 v_{dA}^2 ; \tag{5.33}$$

where, $C_{DC} = q_{d0}/(4\pi\varepsilon_0 m_d R)^{1/2}$. In this limit, the plasma Debye length becomes redundant. It needs a new spatial regime for the DCWs to exist. Let $\lambda_R = a_d\,(a_d/3R\delta)^{1/2}$ be the new scale length known as the modified Wigner-Seitz radius. It signifies the modified dust intergrain separation due to its number density, charge fluctuations and size. It plays a similar role in dense dusty plasmas as $\lambda_{D\kappa}$ in the tenuous plasmas. Now, equation (5.33) can be given as

$$\omega^2 = \left(k^2 + \frac{1}{r^2}\right)\left[\frac{C_{DC}^2}{\delta(1+k^2\lambda_R^2)} + \frac{\gamma_d v_{td}^2}{2} - \frac{\omega_{Jd}^2}{k^2}\right] + k^2 v_{dA}^2. \tag{5.34}$$

Thus, equation (5.34) describes the evolution of the instability dynamics excitable in the considered dusty plasma system in the hydrodynamic regime. Clearly, the dust-fugacity has no direct impact on this fluctuation dynamics significantly except via $\lambda_R = \lambda_D\sqrt{f\delta}$. Besides, the dynamics in the WC regime is fully free from any kind of viscoelastic effects.

As an immediate corollary of equation (5.34), we apply the previous approximation of cold unmagnetized plasma confined in planar geometry. Accordingly, the phase velocity and group velocity of the DCW can be derived from equation (5.34) in the HFR as $(v_{DC})_p = C_{DC}\left[\delta\left(1+k^2\lambda_R^2\right)\right]^{-1/2}$ and $(v_{DC})_g = (v_{DC})_p\left(1+3k^2\lambda_R^2\right)\left(1+k^2\lambda_R^2\right)^{-1}$, respectively. In the long-wavelength limit, the respective modal parameters become $(v_{DC})_p = C_{DA}(\delta)^{-1/2}$ and $(v_{DC})_g = (v_{DC})_p$. Besides, in the short-wavelength limit, the quantities get respectively modified as $(v_{DC})_p = C_{DC}\left[\sqrt{\delta}\,k\lambda_R\right]^{-1}$ and $(v_{DC})_g = 3(v_{DC})_p$. So, the DCW mode, similar to the previous DAW mode in the LFR, is also dispersive in nature in the short-wavelength regime and non-dispersive in the long-wavelength regime with the critical existential spatial scale-length, $\lambda_R$.

In a special planar case with the asymptotic limits of $r \to \infty$, $\kappa_e, \kappa_i \to \infty$, $\lambda_{D\kappa} \to \lambda_D$, and $B_{\varphi 0} = 0$, equations (5.32)-(5.34) retrieve back the linear quadratic dispersion relations, as already reported by Rao and his group [9-13], which are validated only for the WC MB-distributed dusty plasma systems in the tenuous and dense cases presented respectively as

$$\frac{\omega^2}{k^2} = \frac{C_{DA}^2}{(1+k^2\lambda_D^2)} + \frac{\gamma_d v_{td}^2}{2} - \frac{\omega_{Jd}^2}{k^2}, \tag{5.35}$$

$$\frac{\omega^2}{k^2} = \frac{C_{DC}^2}{\delta(1+k^2\lambda_R^2)} + \frac{\gamma_d v_{td}^2}{2} - \frac{\omega_{Jd}^2}{k^2}. \tag{5.36}$$

A close inspection herewith shows that the mathematical constructs of our quadratic dispersion relations (equations (5.35)-(5.36) herein) derived in the hydrodynamic (low-frequency) limit match quite well with those reported in the literature (equations (5.14)-(5.15) in [11]). It hereby fully confirms the reliability testing of our proposed model formalisms and analyses categorically; thereby, making us go ahead in the right direction of the instability dynamics.

b) Kinetic limit:

In the SCL, $\omega\tau_m >> 1$ [30, 31], equation (5.30) transforms as

$$\omega^2 = \left(k^2 + \frac{1}{r^2}\right)\left[\frac{C_{DA}^2}{[1+k^2\lambda_{D\kappa}^2 + f\delta]} + \frac{\gamma_d v_{td}^2}{2} - \frac{\omega_{Jd}^2}{k^2}\right] + k^2 v_{dA}^2 + \frac{1}{m_d n_{d0}\tau_m}\left\{k^2\chi + \frac{2}{r^2}\left(\varsigma + \frac{\eta}{3}\right)\right\}. \quad (5.37)$$

It is to be clearly noted from equation (5.37) that the instability dynamics in our plasma model in the SCL exhibits viscoelastic features relevant in diverse compact astrocosmic environs [44, 45], such as the neutron stars, dwarf stars, planetary disks, planetary interiors, etc. Similarly, in the LFR $f\delta << 1$, and in the HFR $f\delta >> 1$ [9-13], equation (5.37), respectively, reduces to

$$\omega^2 = \left(k^2 + \frac{1}{r^2}\right)\left[\frac{C_{DA}^2}{1+k^2\lambda_{D\kappa}^2} + \frac{\gamma_d v_{td}^2}{2} - \frac{\omega_{Jd}^2}{k^2}\right] + k^2 v_{dA}^2 + \frac{1}{m_d n_{d0}\tau_m}\left\{k^2\chi + \frac{2}{r^2}\left(\varsigma + \frac{\eta}{3}\right)\right\}. \quad (5.38)$$

$$\omega^2 = \left(k^2 + \frac{1}{r^2}\right)\left[\frac{C_{DC}^2}{\delta(1+k^2\lambda_R^2)} + \frac{\gamma_d v_{td}^2}{2} - \frac{\omega_{Jd}^2}{k^2}\right] + k^2 v_{dA}^2 + \frac{1}{m_d n_{d0}\tau_m}\left\{k^2\chi + \frac{2}{r^2}\left(\varsigma + \frac{\eta}{3}\right)\right\}. \quad (5.39)$$

Moreover, in the asymptotic limits as mentioned above ($r \to \infty$, $\kappa_e, \kappa_i \to \infty$, $\lambda_{D\kappa} \to \lambda_D$, and $B_{\varphi 0} = 0$), equations (5.38)-(5.39) yield the linear dispersion relations for SC MB-distributed dusty plasma system both in the LFR and HFR cases given respectively as

$$\frac{\omega^2}{k^2} = \frac{C_{DA}^2}{(1+k^2\lambda_D^2)} + \frac{\gamma_d v_{td}^2}{2} - \frac{\omega_{Jd}^2}{k^2} + \frac{\chi}{m_d n_{d0}\tau_m}, \quad (5.40)$$

$$\frac{\omega^2}{k^2} = \frac{C_{DC}^2}{\delta(1+k^2\lambda_R^2)} + \frac{\gamma_d v_{td}^2}{2} - \frac{\omega_{Jd}^2}{k^2} + \frac{\chi}{m_d n_{d0}\tau_m}. \quad (5.41)$$

The normalized forms of equations (5.32), (5.34)-(5.36), (5.38)-(5.41) previously evolving in the old Fourier space $(k, \omega)$ after a standard astronomical (Jeans) normalization scheme [8, 39, 46] evolved in the new Fourier space $(K, \Omega)$ [8, 39, 46], respectively, cast as

$$\Omega^2 = \left(K^2 + \frac{1}{\xi^2}\right)\left[\frac{1}{(1+K^2K_J^2\lambda_{D\kappa}^2)} + \frac{\gamma_d}{2}\left(\frac{v_{td}}{C_{DA}}\right)^2 - \frac{1}{K^2}\right] + K^2\left(\frac{v_{dA}}{C_{DA}}\right)^2, \tag{5.42}$$

$$\Omega^2 = \left(K^2 + \frac{1}{\xi^2}\right)\left[\frac{(C_{DC}/C_{DA})^2}{\delta(1+K^2K_J^2\lambda_R^2)} + \frac{\gamma_d}{2}\left(\frac{v_{td}}{C_{DA}}\right)^2 - \frac{1}{K^2}\right] + K^2\left(\frac{v_{dA}}{C_{DA}}\right)^2, \tag{5.43}$$

$$\Omega^2 = K^2\left[\frac{1}{(1+K^2K_J^2\lambda_D^2)} + \frac{\gamma_d}{2}\left(\frac{v_{td}}{C_{DA}}\right)^2 - \frac{1}{K^2}\right], \tag{5.44}$$

$$\Omega^2 = K^2\left[\frac{(C_{DC}/C_{DA})^2}{\delta(1+K^2K_J^2\lambda_R^2)} + \frac{\gamma_d}{2}\left(\frac{v_{td}}{C_{DA}}\right)^2 - \frac{1}{K^2}\right], \tag{5.45}$$

$$\Omega^2 = \left(K^2 + \frac{1}{\xi^2}\right)\left[\frac{1}{(1+K^2K_J^2\lambda_{D\kappa}^2)} + \frac{\gamma_d}{2}\left(\frac{v_{td}}{C_{DA}}\right)^2 - \frac{1}{K^2}\right] + K^2\left(\frac{v_{dA}}{C_{DA}}\right)^2 +$$

$$\frac{1}{m_d n_{d0}\tau_m C_{DA}^2}\left\{K^2\chi + \frac{2}{\xi^2}\left(\varsigma + \frac{\eta}{3}\right)\right\}, \tag{5.46}$$

$$\Omega^2 = \left(K^2 + \frac{1}{\xi^2}\right)\left[\frac{(C_{DC}/C_{DA})^2}{\delta(1+K^2K_J^2\lambda_R^2)} + \frac{\gamma_d}{2}\left(\frac{v_{td}}{C_{DA}}\right)^2 - \frac{1}{K^2}\right] + K^2\left(\frac{v_{dA}}{C_{DA}}\right)^2 +$$

$$\frac{1}{m_d n_{d0}\tau_m C_{DA}^2}\left\{K^2\chi + \frac{2}{\xi^2}\left(\varsigma + \frac{\eta}{3}\right)\right\}, \tag{5.47}$$

$$\Omega^2 = K^2\left[\frac{1}{(1+K^2K_J^2\lambda_D^2)} + \frac{\gamma_d}{2}\left(\frac{v_{td}}{C_{DA}}\right)^2 + \frac{\chi}{m_d n_{d0}\tau_m C_{DA}^2} - \frac{1}{K^2}\right], \tag{5.48}$$

$$\Omega^2 = K^2\left[\frac{(C_{DC}/C_{DA})^2}{\delta(1+K^2K_J^2\lambda_R^2)} + \frac{\gamma_d}{2}\left(\frac{v_{td}}{C_{DA}}\right)^2 + \frac{\chi}{m_d n_{d0}\tau_m C_{DA}^2} - \frac{1}{K^2}\right]. \tag{5.49}$$

Here, $\xi = r/\lambda_J$, $\Omega = \omega/\omega_{Jd}$, and $K = k/k_J$ are the Jeans-normalized radial distance, angular frequency, and angular wavenumber, respectively. The various normalizing parameters here are $\omega_{Jd}$, the Jeans scale-length, $\lambda_J = C_{DA}/\omega_{Jd}$ m, and Jeans critical angular wavenumber, $k_J = \omega_{Jd}/C_{DA}$. Clearly, equations (5.42)-(5.49) can be employed to see the dispersive features of the DAW and DCW in both the WCL and SCL.

## 5.3 RESULTS AND DISCUSSIONS

A theoretic model is developed to see the stability of a magnetized viscoelastic three-component spherical charge-fluctuating DMC with non-thermal ( $\kappa-$distributed) electrons and ions in the GH model fabric on the astronomic scales of space and time. It considers the relevant effects of both the non-local gravitational and non-gravitational force fields in a spherically symmetric geometry. Application of spherical wave analysis gives a generalized linear dispersion relation (quadratic equation (5.32)) in the extreme regimes of the dust-fugacity and the electro-thermal coupling (signifying the measure of viscoelasticity). The reduced forms of the dispersion relation are numerically analysed in the WCL (equations (5.42)-(5.43)) and SCL (equations (5.46)-(5.47)). Both the limits are further investigated in the LFR and HFR with an interesting special corollaries to the MB-distributed plasma particles as two distinct realistic sub-cases (equations (5.44)-(5.45) and equations (5.48)-(5.49)). The investigated profile pattern outputs in the wave space are being finally compared and interpreted lucidly.

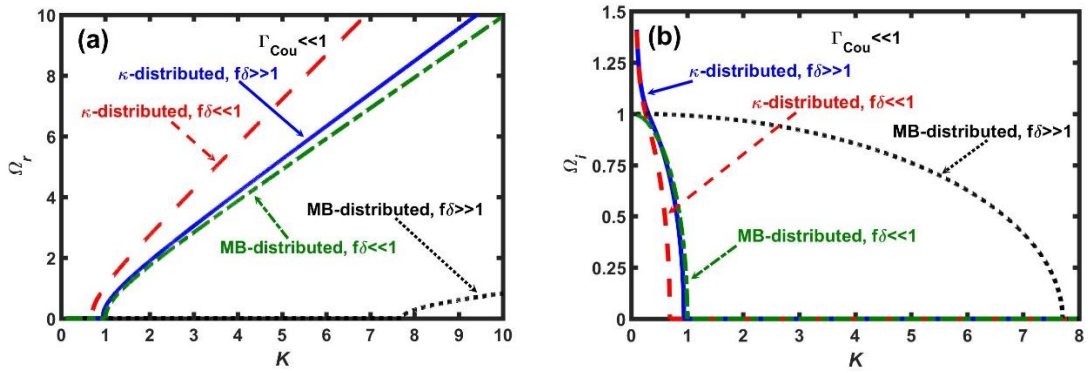


***Figure 5.1:*** *Profile of the Jeans-normalized (a) real frequency* $(\Omega_r)$ *and (b) growth rate* $(\Omega_i)$ *of the composite instability excited in our cloud model with variation in its Jeans-normalized angular wavenumber* $(K)$ *comparing the DCW and DAW modal features illustratively for both the* $\kappa-$*distributed and MB-distributed plasma cases in the weakly coupled regime.*

In figure 5.1, the profile of the Jeans-normalized (a) real frequency $(\Omega_r)$ and (b) growth rate $(\Omega_i)$ with variation in $K$ depicting the DAW and DCW modal features of both the non-thermal ( $\kappa-$case) and thermal (MB-case) plasma particles in the WCL are presented. The corresponding zoomed-in portion is displayed in figure 5.2. Both the non-thermal and thermal cases are further portrayed in the HFR and LFR each therein. The different reliable inputs borrowed from the literature [8, 38, 47-49] are employed in our

analysis. Here, $\xi = 10$, $Z_d = 50$, $n_{e0} = 2 \times 10^5$ m$^{-3}$, $n_{i0} = 4 \times 10^5$ m$^{-3}$, $m_e = 9.1 \times 10^{-31}$ kg, $m_i = 1.67 \times 10^{-27}$ kg, $m_d = 1.86 \times 10^{-16}$ kg [47, 48]; $\varsigma = 10^{-15}$ kg m$^{-1}$ s$^{-1}$, $\eta = 10^{-16}$ kg m$^{-1}$ s$^{-1}$, $\tau_m = 10^{-2}$ s [8, 49]; $\kappa_e = 5.5$, $\kappa_e = 4.7$ [38]; $T_e = 1 \times 10^4$ K, $T_i = 1 \times 10^4$ K, $T_d = 20$ K [47, 48], and $B_{\varphi 0} = 10^{-10}$ T [47]. In this WCL, one estimates $\Gamma_{Cou} = 5.3 \times 10^{-2}$. In the $\kappa-$case for the HFR, we take $R = 10^{-5}$ m to obtain $f = 46.41$, $\lambda_R = 1.15$ m, and $\lambda_{D\kappa} = 7.85$ m, so that the condition for the excitation of the DCWs ($\lambda_R^2 << \lambda_{D\kappa}^2$) is well fulfilled [10]. Conversely, for the LFR, we adopt $R = 10^{-8}$ m to get $f = 4.6 \times 10^{-2}$, $|\lambda_R| = 36.4$ m, and $\lambda_{D\kappa} = 7.85$ m, so that the condition for the excitation of the DAWs ($\lambda_R^2 >> \lambda_{D\kappa}^2$) is well satisfied [10]. Conversely, in the MB-case for the HFR, we estimate $f = 59$, $\lambda_R = 1.15$ m, $\lambda_{D\kappa} = 8.92$ m, and $\lambda_R^2 << \lambda_{D\kappa}^2$. Again, for the LFR, we get $f = 5.9 \times 10^{-2}$, $\lambda_R = 36.41$ m, $\lambda_{D\kappa} = 8.92$ m, and $\lambda_R^2 >> \lambda_{D\kappa}^2$. It is to be noted here that the critical wavenumber ($K_c$) is a transition point in the wave space separating the stable and unstable nature of the fluctuations (growing for $K < K_c$ and propagatory for $K > K_c$). Clearly, for the $\kappa-$case in the HFR ($f\delta >> 1$), one finds $K_c \sim 0.94$ (figure 5.2); and, for the LFR case ($f\delta << 1$), it reads $K_c \sim 0.69$ (figure 5.2). Similar stability features are found to exist in the MB-case as well. Now, in the former ($f\delta >> 1$), we see $K_c \sim 7.8$ (figure 5.1); and, $K_c \sim 1$ (figure 5.1) for the latter ($f\delta << 1$). This interestingly means that the long-wavelength (gravitational, $K \to 0$) fluctuations become more unstable in both the LFR and HFR of the $\kappa-$case and LFR of the MB-case. In contrast, the short-wavelength (acoustic, $K \to \infty$) fluctuations become unstable only in the HFR of the MB-case. It is to be noted that, $K_c$ for both the modes with the MB-case supersedes those in the $\kappa-$case. In the MB-case, however, $K_c$ for the dense system (HFR) gets shifted sharply against its tenuous counterpart (LFR). The $K_c$-shift in the $\kappa-$case is very less in comparison with the MB-case. It is seen here that, in both the plasma special cases, $K_c$ increases with the system compactness (fugacity effects). But, in the $\kappa-$case, the presence of the superthermal electrons and ions increase the randomizing non-thermal pressure force. The lighter species get stuck to the dust surface more rapidly, resulting in an enhanced mutual dust-dust Coulombic force. As a consequence, the net outward pressure force in a $\kappa-$case is more than that in the MB-case. The magnitudes of $\Omega_r$ and $\Omega_i$ are higher in the $\kappa-$case than the

MB-counterparts. So, the $\kappa-$case of the DMC gets destabilized more powerfully and more rapidly than the MB-moderated conjectures.

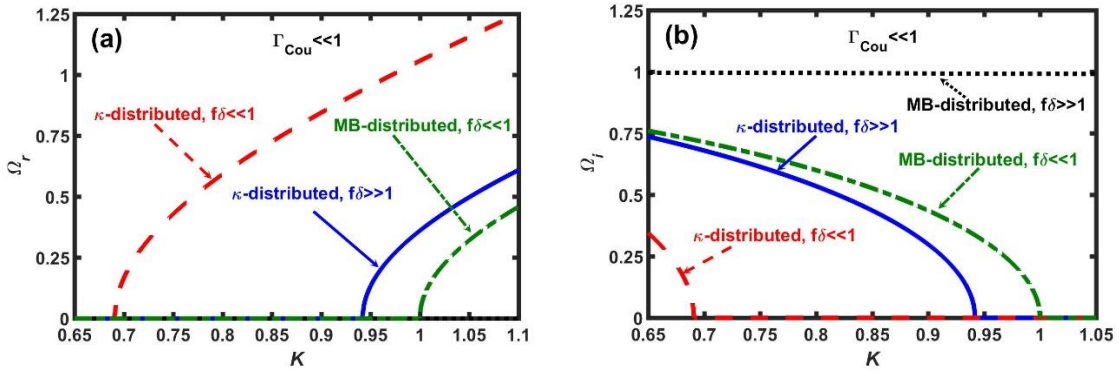


***Figure 5.2:*** *Same as figure 5.1, but in the zoomed form to depict the $K$-criticalities clearly.*

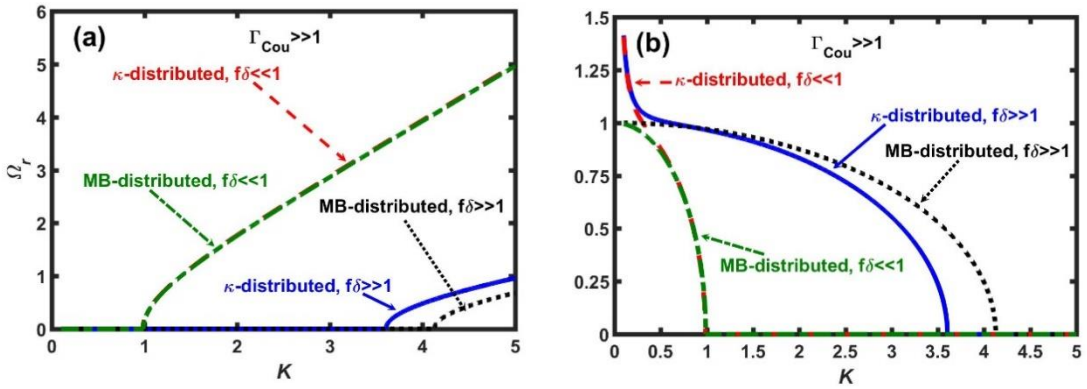


***Figure 5.3:*** *Same as figure 5.1, but in the strongly coupled regime.*

In figure 5.3, we display the same as figure 5.1, but in the SCL. The new input values, apart from figure 5.1, are $Z_d = 10^3$, $n_{i0} = 4\times10^8$ m$^{-3}$, $n_{e0} = 2\times10^8$ m$^{-3}$, and $\Gamma_{Cou} = 78.61$. In the $\kappa-$case, for the HFR, we take $R = 10^{-4}$ m, so that $f = 23.21$, $\lambda_R = 5.15\times10^{-2}$ m, $\lambda_{D\kappa} = 2.48\times10^{-1}$ m, and $\lambda_R^2 << \lambda_{D\kappa}^2$ [10]. For the LFR, we adopt $R = 10^{-7}$ m to obtain $f = 2.32\times10^{-2}$, $|\lambda_R| = 4.8\times10^{-1}$ m, $\lambda_{D\kappa} = 2.5\times10^{-1}$ m, and $\lambda_R^2 >> \lambda_{D\kappa}^2$ [10]. In the MB-case, for the HFR, we estimate $f = 29.98$, $\lambda_R = 5.15\times10^{-2}$ m, $\lambda_{D\kappa} = 2.82\times10^{-1}$ m, and $\lambda_R^2 << \lambda_{D\kappa}^2$. Again, for the LFR, we get $f = 3.0\times10^{-2}$, $\lambda_R = 1.63$ m, $\lambda_{D\kappa} = 2.82\times10^{-1}$ m, and $\lambda_R^2 >> \lambda_{D\kappa}^2$. In the $\kappa-$case of the SCL, it is found that $K_c$ increases for both the HFR ($K_c \sim 3.6$) and the LFR ($K_c \sim 0.98$) against the WCL (figure 5.4). But in the MB-case, $K_c$ decreases for both the HFR ($K_c \sim 4.1$) and the LFR (

$K_c \sim 0.99$) (figure 5.4). This is due to the role of the viscoelastic force arising from the collective cooperative dynamics of the dust grains in the $\kappa-$case against the MB-case. In the $\kappa-$case (MB-case), the viscoelastic force is directed inward (outward). It results in enhancing (reducing) the resultant inward gravitational action. As a consequence, the DMC is destabilized (stabilized) in the $\kappa-$case (MB-case) against the non-local gravitational cloud collapse dynamics. It can be hereby inferred that the DAW (DCW) mode is excited at the low (high) *K*-value in both the $\kappa-$MB cases of the SCL. It is furthermore seen that the long-(short-)wavelength fluctuations evolve in the LFR (HFR) in both the $\kappa-$MB cases. The basic physical insight behind this atypical DMC thermostatistical dynamics with conjugational viscoelastic effects could be attributable to the operative transition from a non-uniform non-gravitational pressure (inhomogeneous non-equilibrium, $\kappa-$case) to a uniform non-gravitational one (homogeneous equilibrium, MB-case) in a collective cooperative manner.

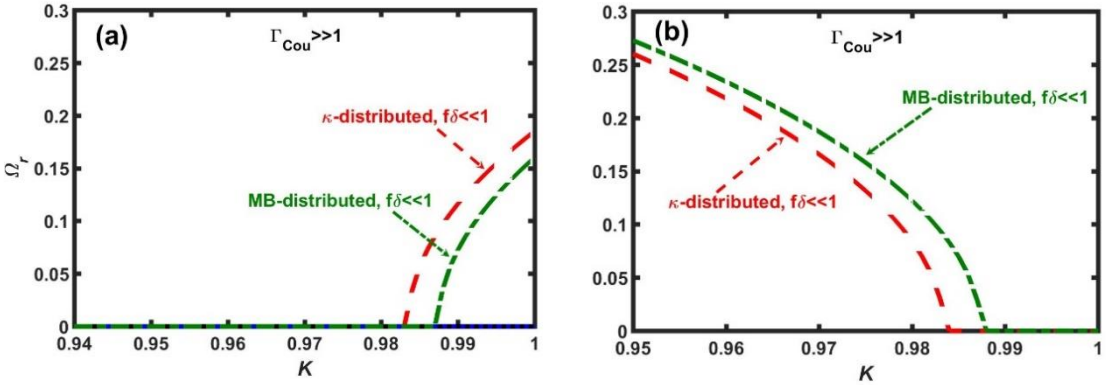


***Figure 5.4:*** *Same as figure 5.3, but in the zoomed form to depict the $K$-criticalities clearly.*

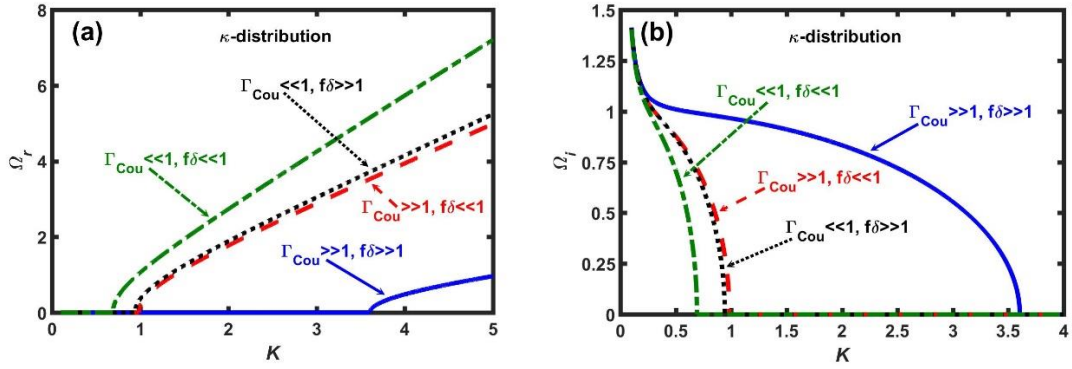


***Figure 5.5:*** *Same as figure 5.1, but in the WCL and SCL of the $\kappa-$distributed plasma case.*

As in figure 5.5, we depict the same as figure 5.1, but in the WCL and SCL of the $\kappa-$case only. It is found that the DAW mode propagates at a high *K*-value ($K_c \sim 3.6$) of the SCL and at a low *K*-value ($K_c \sim 0.94$) of the WCL. The DCW mode get excited at a low *K*-value ($K_c \sim 0.98$) of the SCL and at an ultralow *K*-value ($K_c \sim 0.69$) of the WCL. Thus, the long-wavelength fluctuations occur in the LFR of the SCL; but, in both the LFR and HFR of the WCL. The short-wavelength fluctuations interestingly occur at the HFR of the SCL only (figure 5.5). It is seen further that the DAW and DCW modes in the WCL are excited at a lower *K*-value than its SCL counterpart (figure 5.6). In both the limits, $K_c$ increases with the compactness. So, the strength of the inward gravitational force increases with the compactness, and vice-versa. It is noted that the $K_c$-shift in the SCL is more than that in the WCL. This difference is because of the higher dust population (viscoelastic and strongly gravitating) in the SCL than the opposite rarer counterpart WCL (non-viscoelastic and weakly gravitating). The viscoelastic force in the $\kappa-$case is inward. The conjoint action of the viscoelastic and gravitational forces dominates over the dust-dust Coulomb repulsion in the SCL against the WCL. So, the SC fluids get more destabilized than the WC fluids against the non-local inward gravity in the $\kappa-$case.

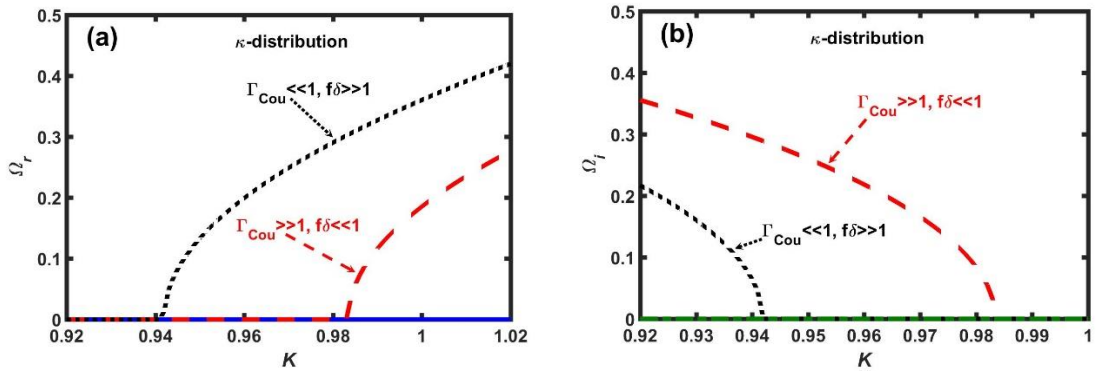


***Figure 5.6:*** *Same as figure 5.4, but in the zoomed form to depict the $K$-criticalities clearly.*

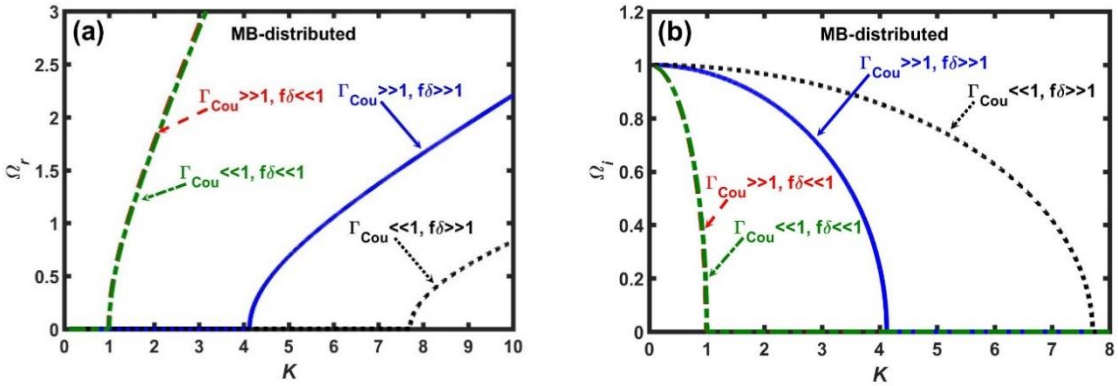


***Figure 5.7:*** *Same as figure 5.5, but in the MB-distributed plasma case.*

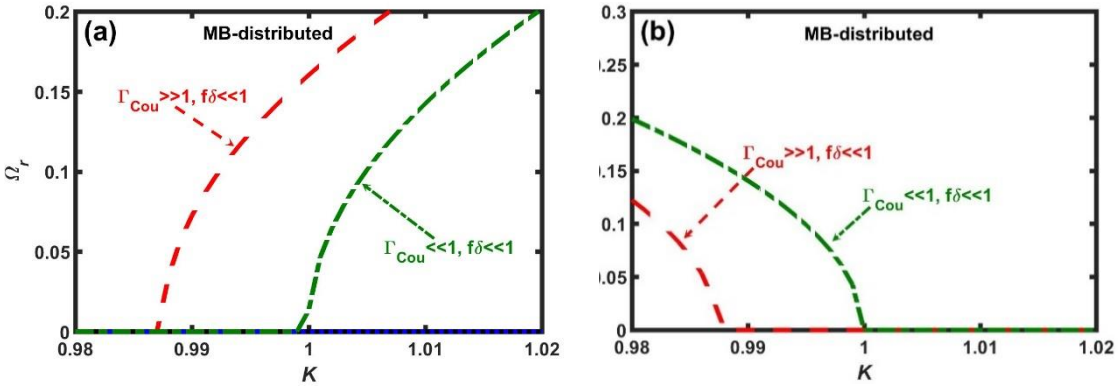


***Figure 5.8:*** *Same as figure 5.7, but in the zoomed form to depict the* $K$ *-criticalities clearly.*

In figure 5.7, we display the same as figure 5.5, but now in the MB-case, alongside the zoomed-in portion displayed in figure 5.8. It is found that the DAW mode occurs at a high *K*-value ( $K_c \sim 4.1$) of the SCL and at an ultrahigh *K*-value ( $K_c \sim 7.8$) of the WCL. Moreover, the DCW mode excitation occurs at a low *K*-value in both the SCL ( $K_c \sim 0.99$ ) and WCL ( $K_c \sim 1$). Hence, the long-(short-) wavelength fluctuations occur in the LFR (HFR) in both the limits of the MB-case. Moreover, the DAW and DCW modes in the WCL evolve at a higher *K*-value than its SCL counterpart. In both the coupling limits, $K_c$ increases with the system compactness, and vice-versa. Here too, the inward organising gravitational force increases with the compactness, and vice-versa. Again, the $K_c$-shift in the SCL is less than that in the WCL (figure 5.8). The viscoelastic force in the MB-case is outward against that acting inward in the $\kappa-$case. The self-gravitational action (inward) is weaker than the conjoint action (outward) of the viscoelastic and dust-dust Coulombic repulsion forces in the SCL against the WCL. It, hereby, displays a mutualistically opposite picture. So, the WC fluids are more destabilized than the SC fluids in the MB-case against the canonical self-gravitational collapse dynamics.

In figure 5.9, we display the same as figure 5.1, but for the different $Z_d$ - values. It is seen that, with an increase in $Z_d$, the magnitude of $\Omega_r$ increases; but the magnitude of $\Omega_i$ decreases; and vice-versa. It means that with an increase in $Z_d$ in the HFR, the Coulombic interaction among the dust grains increases, thereby opposing the inward gravitational pull. Thus, $Z_d$ acts as a stabilizing and accelerating agency of the DMC against the inward collapse.

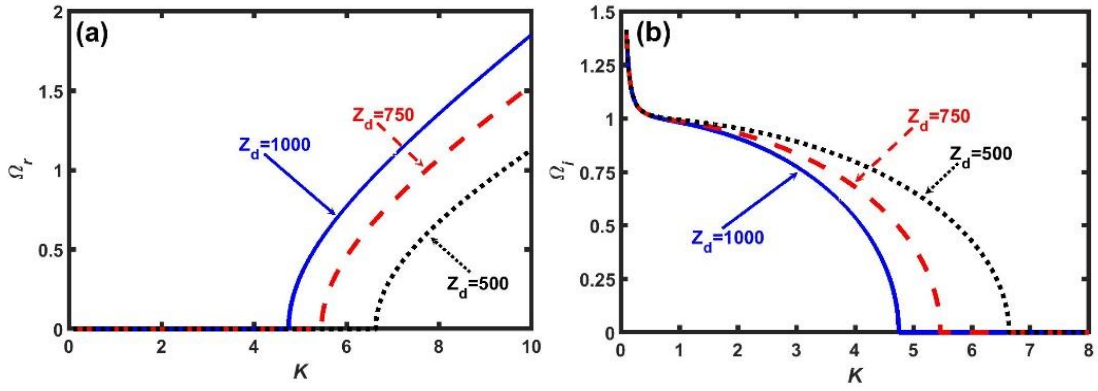


***Figure 5.9:*** *Same as figure 5.1, but for the different* $Z_d$ *- values.*

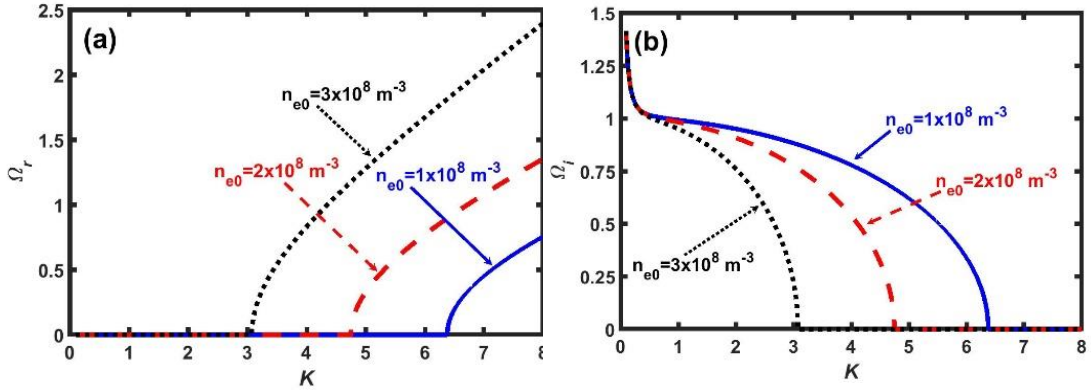


***Figure 5.10:*** *Same as figure 5.1, but for the different* $n_{e0}$ *- values.*

In figure 5.10, we portray the same as figure 5.1, but for the different $n_{e0}$ - values. It is seen that, with an increase in $n_{e0}$, the modal patterns exhibit the similar behaviours as figure 5.9. An enhancement in $n_{e0}$ makes the electron flux current increase. It causes the negative charge of the dust grains to go higher. It, in turn, increases the mutualistic Coulombic repulsion among the grains. As a result, the outward repulsive force overcomes inward gravitational force. Thus, $n_{e0}$ acts as a stabilizing and accelerating agency to the considered DMC.

In figure 5.11, we show the same as figure 5.1, but for the different $n_{i0}$ - values. It is seen that with increase in $n_{i0}$, the profile patterns show an opposite behaviour in contrast to figure 5.9. This means that with an increase in $n_{i0}$, the ion current flux onto the dust surface increases, and vice-versa. It reduces the negative charge of the constituent dust grains. As a result, the strength of the Coulombic repulsion among the grains decreases. It

allows the gravitational force to dominate over the net outward repulsive force of the electrostatic origin. We can, therefore, infer that $n_{i0}$ acts as a destabilizing and decelerating agency of the perturbed DMC against the inward self-gravitational collapse.

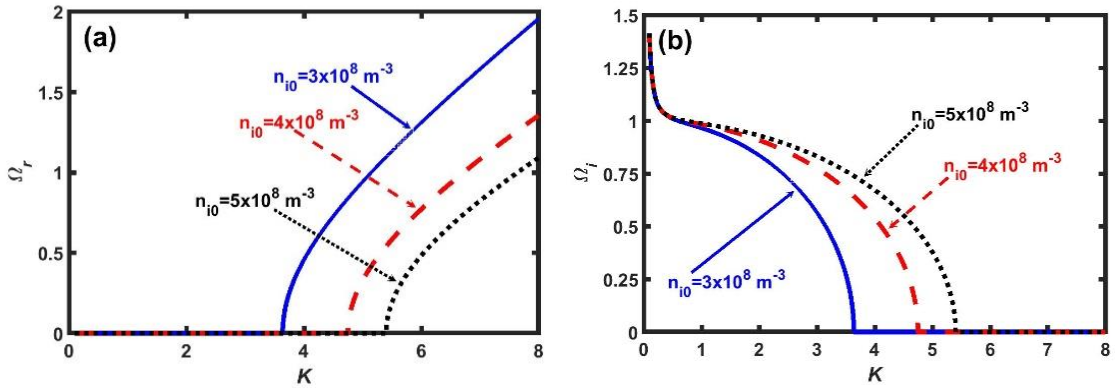


***Figure 5.11:*** *Same as figure 5.1, but for the different* $n_{i0}$ *- values.*

As in figure 5.12, we show the same as figure 5.1, but for the different $B_{\varphi 0}$ - values. Clearly, it shows a similar type of patterns as in figure 5.1. It means that the $B_{\varphi 0}$ acts as a stabilizing and accelerating agent to the dynamics of the fluctuating DMC against the canonical Jeans collapse. It is attributable to the well-known fact that with an increase in $B_{\varphi 0}$, the constituent charged particles get frozen along the magnetic field lines, thereby halting the cloud collapse to grow.

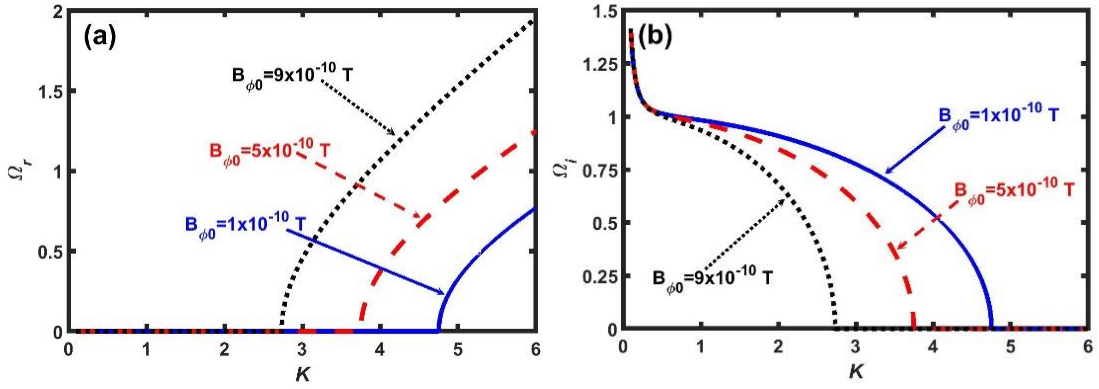


***Figure 5.12:*** *Same as figure 5.1, but for the different* $B_{\varphi 0}$ *- values.*

In figures 5.13-5.14, we display the same as figure 5.1, but for the different $\kappa_e$ - and $\kappa_i$ - values, respectively. It, on an average, follows a similar type of patterns as already

depicted in figure 5.11. We see herewith that, with an increase in $\kappa_e$ ($\kappa_i$), the cloud thermostatistics moves from the superthermality limit (high-energy regime) towards the MB-distribution limit (low-energy regime), and vice-versa. In other words, it means that, with an increase in $\kappa_e$ ($\kappa_i$), the number density of the superthermal plasma particles significantly decreases [38]. As a result, the Coulombic force among the dust grains arising due to the sticking effects of the constitutive plasma particles decreases. This, in turn, makes the inward gravitational force (organizing) to supersede the outward pressure force (randomizing). Thus, it is conclusively inferred that the non-thermality (or superthermality) parameters act as destabilizing and decelerating agent to the DMC fluctuations dynamics against the canonical self-gravity in the non-planar framework of spherical geometry. It may be pertinent to mention here that this destabilizing nature of $\kappa_e$ ($\kappa_i$) in our non-planar complex cloud model is against the previous findings reporting the stabilizing nature of $\kappa_e$ ($\kappa_i$) for the hybrid gravito-acoustic (pulsational) mode in the planar geometry approximation [38, 50]. It hereby confirms that the polarity of the instability dynamics of the non-thermal DMCs is drastically influenced with the uncommon geometric curvature effects alongside minor moderations contributed from the common collective correlative factors associated with the adopted fluid model configurations.

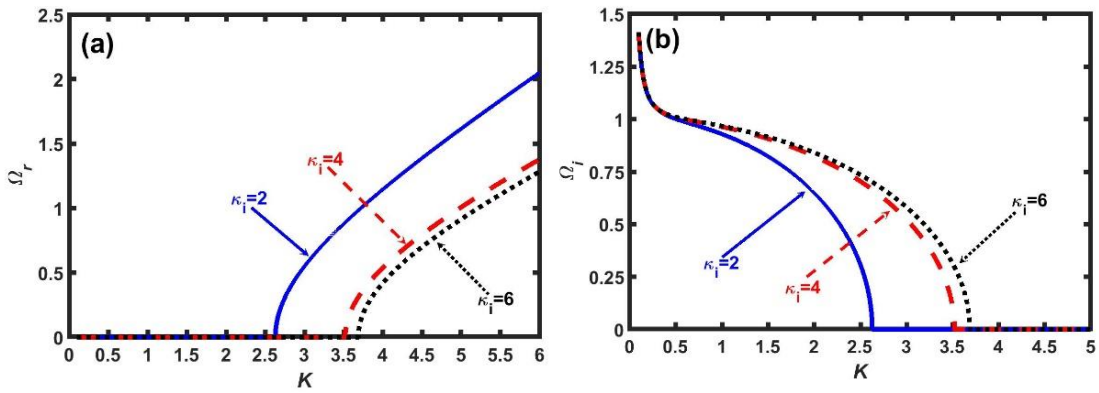


***Figure 5.13:*** *Same as figure 5.1, but for the different* $\kappa_e$ *- values.*

In figure 5.15, we portray the same as figure 5.1, but for the different $\xi$ - values. It herewith shows a unique pattern feature in comparison with the other relevant parameters of the system. Any simultaneous existence of both the propagatory and growth features of the fluctuations are not supported in the DMC system. At $K_c \sim 3.6$, it makes a transition forming a purely growing mode into a propagatory one (i.e. towards the high-frequency

(acoustic) regime). It does not affect $\Omega_r$ -evolution at all (figure 5.15(a)). Moreover, the $\Omega_i$ -variation occurs only at the ultra-low *K*-limit (figure 5.15(b)). In other words, only the long wavelength (gravitational) fluctuations get perturbatively unstable. It is seen that, with an increase in $\xi$, $\Omega_i$ decreases, and vice-versa. Thus, $\xi$ acts as a stabilizer against the inward self-gravity. It is due to the universal inverse square Newtonian law of the long-range self-gravity (cloud-centric), which decreases with the interparticle separation in a given thermodynamic environ. It means that the self-gravitational pressure force in the cloud decreases with increase in the cloud size, and vice-versa. Such stabilizing effects caused by the geometric curvature radius (i.e., deviation from the plane-parallel geometry) are quite bolstered with the previous predictions in similar isothermal gaseous spherical shells [8, 51]. A compact summary of the results investigated here are shown in Table 5.1 and Table 5.2 (in Appendix-5.A) portray the distinctive features of the DAW-DCW and WCL-SCL aspects in DMCs, respectively.

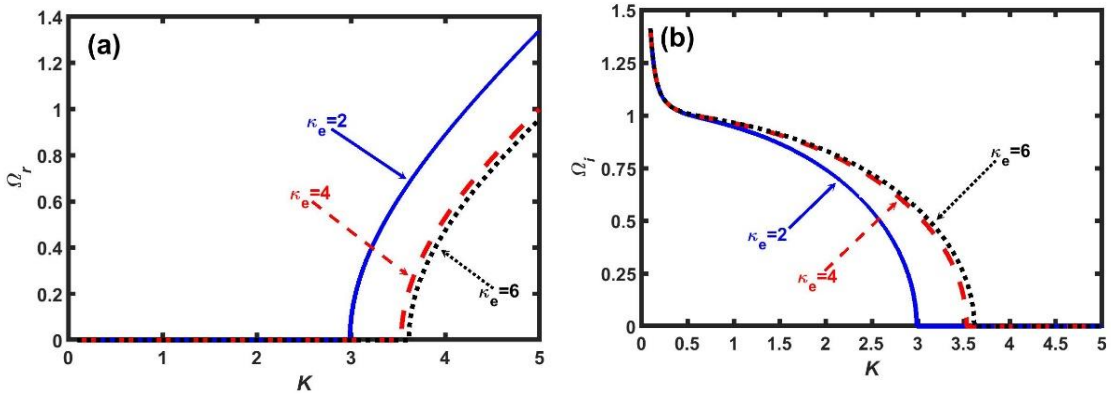


***Figure 5.14:*** *Same as figure 5.1, but for the different* $\kappa_i$ *- values.*

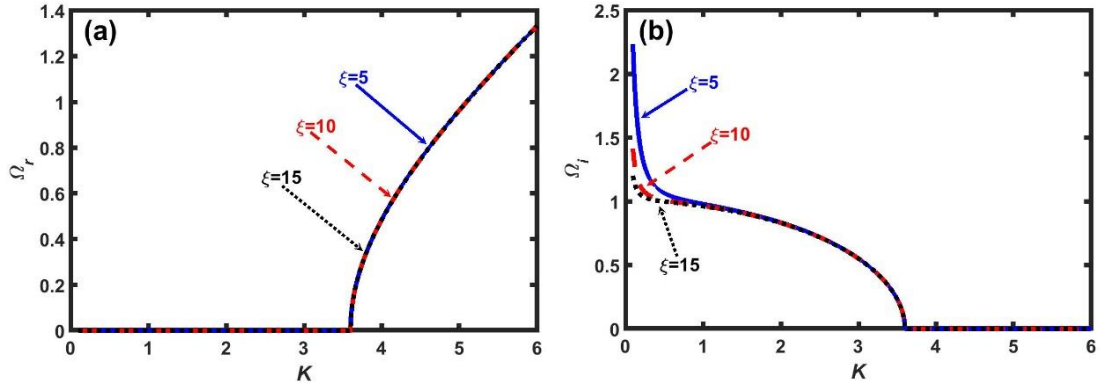


***Figure 5.15:*** *Same as figure 5.1, but for the different* $\xi$ *- values.*

The above analyses on the spherical magnetized DMC can be helpful in understanding the star formation dynamical processes in the RCW 38 region of the dark DMCs. The RCW 38 is a bright $H_{II}$ region having a young, massive star cluster located at a distance of 1.7 kpc away from the Earth in the direction of the constellation Vela [52]. It is observed through the Very Large Telescope in the near-infrared spectral zone [52]. A good number of astronomic observations on the Zeeman effect in such RCW 38-like regions has been previously reported in the literature to correlate the stability of the self-gravitating cloud with its geometry [37]. It has been found that the azimuthal magnetic flux-to-mass ratio in such clouds is $\Phi_B / M_{DMC} = 0.9$ for spherical shape (non-planar, super-critical) and $\Phi_B / M_{DMC} = 1.6$ for sheet-like (planar, sub-critical) geometries [37]. It, thereby, implies that the RCW 38 region is magnetically supercritical and geometrically spherical [37]. As the density of the RCW 38 is twice of Orion nebula cluster, and an order of magnitude denser than other nearby star-forming regions, it may provide a supportive environs for the DCW excitation in the RCW 38 and like regions.

## 5. CONCLUSIONS

This Chapter reports a GH model of gravito-magnetically bounded spherical DMCs to study the excitation of the DAW and DCW in diversified extreme cloud conditions on the Jeans scales of space and time. It includes mainly the effects of non-local self-gravity, non-thermal pressure, and local dust-charge fluctuations in spherical geometry. The dust-charge evolves as a dynamic variable because of the dynamicity of the dependent plasma parameters. Application of a standard spherical wave analysis with no quasi-classic eikonal approximation yields a generalized linear quadratic dispersion relation. It involves an atypical set of multi-parametric coefficients in the wave space sensitively reducible in the extreme regimes of the dust-fugacity and viscoelasticity. The reduced forms of the dispersion relation are numerically analysed in both the WCL and SCL. Both the limits are further investigated in the LFR and HFR. The analysis depicts that both the LFR mode (DAW) and HFR mode (DCW) are dispersive in the short-wavelength (acoustic) regime and non-dispersive in the long-wavelength (gravitational) regime propagating with their respective distinct critical existential scales. An interesting pair of special corollaries relating to the MB-distributed plasma particles as two distinct realistic sub-cases are drawn. The DMC in the WCL is fully free from any kind of viscoelastic effects due to the absence of collective cooperative degrees of freedom. In contrast, the SC fluid exhibits

viscoelasticity due to the presence of collective cooperative degrees of freedom. Such SC fluids are mostly relevant in diverse compact astrostructures and their circumvent atmospheres including planetary magnetospheres, $H_{II}$ regions in DMCs, Saturian rings, etc.

A comparative analysis between the $\kappa-$case and MB-case, and between the SCL and WCL is graphically presented to reveal the physical insights in such hybrid wave-dynamical aspects. In the $\kappa-$case, the long-wavelength (gravitational) fluctuations (Jeansian) are more unstable. It destabilizes the DMCs more strongly and rapidly than its MB-counterparts. The outward Coulombic force among the dust grains dominates more in the $\kappa-$case than in the MB due to superthermality effects. Again, the viscoelastic force is directed inward (outward) in the $\kappa-$case (MB-case). It is conjectured that in the $\kappa-$case (MB-case), in the SCL (WCL) fluids are more destabilized than the corresponding regimes of the WCL (SCL).

In addition to the above mention points, a judicious numerical analysis is performed to explore various stabilizing and destabilizing agents of the fluctuation in the HFR of the SC fluid having $\kappa-$distribution. This investigation enables us to show that the equilibrium dust charge number ($Z_{d0}$), equilibrium electronic population density ($n_{e0}$), and equilibrium azimuthal magnetic field ($B_{\varphi 0}$) act as stabilizing and accelerating agencies to the fluctuation dynamics. Conversely, the equilibrium ionic population density ($n_{i0}$), non-thermality parameter ($\kappa_e$ and $\kappa_i$) act as destabilizing and decelerating agents against self-gravity effects.

An interesting outcome here is that the polarity of the instability dynamics of the non-thermal DMCs is drastically influenced with the uncommon geometric curvature effects alongside minor moderations contributed from the common collective correlative factors associated with the adopted fluid model. In a broader sense, the non-thermality parameters plays as a destabilizer (stabilizer) in the non-planar (planar) geometry. It is to be further noted that the cloud dimension ($\xi$) adds a unique feature to the fluctuation dynamics. It acts as a stabilizer in the ultra-low *K* only; but, plays no role in accelerating/decelerating the DMC fluid.

The scale-invariant (normalized) bimodal instability evolutionary features, particularly on the DCW dynamics as explored here, are found to be consistent with the experimental observations reported on the laboratory scales of space and time [14]. On the astrophysical scales too, the proposed semi-analytic model formalism can have potential applications to understand diversified structure formation mechanisms as discussed above.

## REFERENCES


[1] Kutner, M. L. *Astronomy: A Physical Perspective.* Cambridge University Press, Cambridge, 2003.

[2] Liseau, R., Larsson, B., Lunttila, T., Olberg, M., Rydbeck, G., Bergman, P., Justtanont, K., Olofsson, G., and de Vries, B. L. Gas and dust in the star-forming region ρ Oph A-The dust opacity exponent β and the gas-to-dust mass ratio g2d. *Astronomy & Astrophysics,* 578: A131. 1-21, 2015.

[3] Tricco, T. S., Price, D. J., and Laibe, G. Is the dust-to-gas ratio constant in molecular clouds? *Monthly Notices of the Royal Astronomical Society,* 471: L52-L56, 2017.

[4] Popel, S. I. and Tsytovich, V. N. Shocks in space dusty plasmas. *Astrophysics and Space Science,* 264: 219-226, 1998.

[5] Popel, S. I., Tsytovich, V. N., and Yu, M. Y. Shock structures in plasmas containing variable-charge macro particles. *Astrophysics and Space Science,* 256: 107-123, 1997.

[6] Popel, S. I. and Gisko, A. A. Charged dust and shock phenomena in the solar system. *Nonlinear Processes in Geophysics,* 13: 223-229, 2006.

[7] Bellan, P. M. Enrichment of the dust-to-gas mass ratio in Bondi/Jeans accretion/cloud systems due to unequal changes in dust and gas incoming velocities. *Astrophysical Journal,* 678: 1099-1108, 2008.

[8] Kalita, D. and Karmakar, P. K. Analyzing the instability dynamics of spherical complex astroclouds in a magnetized meanfluidic fabric. *Physics of Plasmas,* 27: 022902. 1-16, 2020.

[9] Rao, N. N. Dust–Coulomb waves in dense dusty plasmas. *Physics of Plasmas,* 6: 4414-4417, 1999.

[10] Rao, N. N. Dust-Coulomb and dust-acoustic wave propagation in dense dusty plasmas with high fugacity. *Physics of Plasmas,* 7: 795-807, 2000.

[11] Rao, N. N. and Verheest, F. Electrostatic dust modes in self-gravitating dense dusty plasmas with high fugacity. *Physics Letters A,* 268: 390-394, 2000.

[12] Rao, N. N. Electrostatic modes in dense dusty plasmas with high fugacity: Numerical results. *Physics of Plasmas,* 7: 3214-3226, 2000.

[13] Rao, N. N. Electrostatic waves in dense dusty plasmas with high fugacity. *Physica Scripta,* T89: 176-182, 2001.

[14] Nunomura, S., Misawa, T., Ohno, N., and Takamura, S. Instability of dust particles in a coulomb crystal due to delayed charging. *Physical Review Letters,* 83: 1970-1973, 1999.

[15] Tolba, R. E. Propagation of dust-acoustic nonlinear waves in a superthermal collisional magnetized dusty plasma. *European Physical Journal Plus,* 136: 138. 1-15, 2021.

[16] Livadiotis, G. and McComas, D. J. Exploring transitions of space plasmas out of equilibrium. *Astrophysical Journal,* 714: 971-987, 2010.

[17] Livadiotis, G. and McComas, D. J. Understanding kappa distributions: A toolbox for space science and astrophysics. *Space Science Reviews,* 175: 183-214, 2013.

[18] Vasyliunas, V. M. A survey of low-energy electrons in the evening sector of the magnetosphere with OGO 1 and OGO 3. *Journal of Geophysical Research,* 73: 2839-2884, 1968.

[19] Leubner, M. P. and Vörös, Z. A nonextensive entropy approach to solar wind intermittency. *Astrophysical Journal,* 618: 547-555, 2005.

[20] Yoon, P. H., Rhee, T., and Ryu, C.-M. Self-consistent formation of electron κ distribution: 1. Theory. *Journal of Geophysical Research,* 111: A09106. 1-10, 2006.

[21] Pierrard, V. and Lazar, M. Kappa distributions: Theory and applications in space plasmas. *Solar Physics,* 267: 153-174, 2010.

[22] Goutam, H. P. and Karmakar, P. K. Turbulent Gravito-Electrostatic Sheath (GES) structure with kappa-distributed electrons for solar plasma characterization. *Solar Physics,* 292: 182. 1-12, 2017.

[23] Christon, S. P. A comparison of the Mercury and Earth magnetospheres: Electron measurements and substorm time scales. *Icarus,* 71: 448-471, 1987.

[24] Mauk, B. H., Mitchell, D. G., McEntire, R. W., Paranicas, C. P., Roelof, E. C., Williams, D. J., Krimigis, S. M, and Lagg, A. Energetic ion characteristics and neutral gas interactions in Jupiter's magnetosphere. *Journal of Geophysical Research,* 109: A09S12. 1-24 2004.

[25] Dialynas, K., Krimigis, S. M., Mitchell, D. G., Hamilton, D. C., Krupp, N., and Brandt, P. C. Energetic ion spectral characteristics in the Saturnian magnetosphere using Cassini/MIMI measurements. *Journal of Geophysical Research,* 114: A01212, 1-7, 2009.

[26] Decker, R. B. and Krimigis, S. M. Voyager observations of low-energy ions during solar cycle 23. *Advances in Space Research,* 32: 597-602, 2003.

[27] Decker, R. B., Krimigis, S. M., Roelof, E. C., Hill, M. E., Armstrong, T. P., Gloeckler, G., Hamilton, D. C., and Lanzerotti, L. J. Voyager 1 in the foreshock, termination shock, and heliosheath. *Science,* 309: 2020-2024, 2005.

[28] Livadiotis, G., McComas, D. J., Dayeh, M. A., Funsten, H. O., and Schwadron, N. A. First sky map of the inner heliosheath temperature using IBEX spectra. *Astrophysical Journal,* 734: 1-19, 2011.

[29] Nicholls, D. C., Dopita, M. A., and Sutherland, R. S. Resolving the electron temperature discrepancies in H II regions and planetary nebulae: κ-distributed electrons. *Astrophysical Journal,* 752: 148. 1-16, 2012.

[30] Karmakar, P. K. and Das, P. Stability of gravito-coupled complex gyratory astrofluids. *Astrophysics and Space Science,* 362: 115. 1-9, 2017.

[31] Das, P. and Karmakar, P. K. Dynamics of flow-induced instability in gyrogravitating complex viscoelastic quantum fluids. *AIP Advances,* 8: 085209. 1-14, 2018.

[32] Shu, F. H. Ambipolar diffusion in self-gravitating isothermal layers. *Astrophysical Journal,* 273: 202-213, 1983.

[33] Paleologou, E. V. and Mouschovias, T. C. The magnetic flux problem and ambipolar diffusion during star formation-One-dimensional collapse. I-Formulation of the problem and method of solution. *Astrophysical Journal,* 275: 838-857, 1983.

[34] Mouschovias, T. C. and Morton, S. A. Ambipolar diffusion, cloud cores, and star formation: Two-dimensional, cylindrically symmetric contraction. I-The issues, formulation of the problem, and method of solution. *Astrophysical Journal,* 371: 296-316, 1991.

[35] Mouschovias, T. C. Magnetic braking, ambipolar diffusion, cloud cores, and star formation-Natural length scales and protostellar masses. *Astrophysical Journal,* 373: 169-186, 1991.

[36] Safier, P. N., McKee, C. F., and Stahler, S. W. Star formation in cold, spherical, magnetized molecular clouds. *Astrophysical Journal,* 485: 660-679, 1997.

[37] Bourke, T. L., Myers, P. C., Robinson, G., and Hyland, A. R. New OH Zeeman measurements of magnetic field strengths in molecular clouds. *Astrophysical Journal,* 554: 916-932, 2001.

[38] Pajouh, H. H. and Afshari, N. Influence of superthermal plasma particles on the Jeans instability in self-gravitating dusty plasmas with dust charge variations. *Physics Letters A,* 380: 3810-3816, 2016.

[39] Karmakar, P. K. and Kalita, D., Dynamics of gravitational instability excitation in viscoelastic polytropic fluids. *Astrophysics and Space Science,* 363: 239. 1-11, 2018.

[40] de Juli, M. C., Schneide, R. S., Ziebell, L. F., and Gaelzer, R. Effects of dust charge variation on electrostatic waves in dusty plasmas with temperature anisotropy. *Brazilian Journal of Physics,* 39: 112-133, 2009.

[41] Tsytovich, V. N., Sato, N., and Morfill, G. E. Note on the charging and spinning of dust particles in complex plasmas in a strong magnetic field. *New Journal of Physics,* 5: 43. 1-9, 2003.

[42] Draine, B. T. *Physics of the Interstellar and Intergalactic medium.* Princeton University Press, Princeton, 2010.

[43] Elmore, W. C., and Heald M. A., *Physics of Waves*. Dover, New York, 1969.

[44] Bastrukov, S. I., Weber, F., and Podgainy, D. V. On the stability of global non-radial pulsations of neutron stars. *Journal of Physics G: Nuclear and Particle Physics,* 25: 107-127, 1999.

[45] Verheest, F. *Waves in Dusty Space Plasmas.* Kluwer Academic Publishers, London, 2000.

[46] Kalita, D. and Karmakar, P. K., Nonlinear dynamics of gravitational instability in complex viscoelastic astrofluids. *AIP Advances,* 8: 085207. 1-15, 2018.

[47] Spitzer Jr, L. *Physical Processes in the Interstellar Medium.* Wiley, New York, 2004.

[48] Pandey, B. P., Vranješ, J., Poedts, S., and Shukla, P. K. The pulsational mode in the presence of dust charge fluctuations. *Physica Scripta,* 65: 513-517, 2002.

[49] Vieillefosse, P. and Hansen, J. P. Statistical mechanics of dense ionized matter. v. hydrodynamic limit and transport coefficients of the classical one-component plasma. *Physical Review A,* 12: 1106-1116, 1975.

[50] Karmakar, P. K. and Dutta, P. Evolutionary pulsational mode dynamics in nonthermal turbulent viscous astrofluids. *Astrophysics and Space Science,* 362: 203. 1-8, 2017.

[51] Tomisaka, K. and Ikeuchi, S. Gravitational instability of isothermal gas layers-Effect of curvature and magnetic field. *Publications of the Astronomical Society of Japan*, 35: 187-208, 1983.

[52] Mužić, K., Schödel, R., Scholz, A., Geers, V. C., Jayawardhana, R., Ascenso, J., and Cieza, L. A. The low-mass content of the massive young star cluster RCW 38. *Monthly Notices of the Royal Astronomical Society*, 471: 3699-3712, 2017.

**APPENDIX-5.A**

Table 5.1: DCW versus DAW

| S. No. | Item | DAW | DCW | Reference |
|---|---|---|---|---|
| 1 | Critical spatial scale | Debye screening length ($\lambda_D$) | Modified Wigner-Seitz radius ($\lambda_R$) | [9-13] |
| 2 | Condition | $\lvert\lambda_{D\kappa}/\lambda_R\rvert >> 1$ | $\lvert\lambda_{D\kappa}/\lambda_R\rvert << 1$ | [10] |
| 3 | Coupling parameter | $\Gamma_{Cou} << 1$ | $\Gamma_{Cou} \leq 1, >> 1$ | [10, 13, 14] |
| 4 | Charge fluctuations | May be zero | Must be non-zero | [9-13] |
| 5 | Fugacity | Tenuous ( $f << 1$) | Dense ( $f >> 1$) | [9-13] |
| 6 | Dust-charge | Low | High | [9, 10] |
| 7 | Dust radius | Small | Large | [10] |
| 8 | Perturbations (generic notations) | $\lvert q_{d0} n_{d1}\rvert \approx \lvert e(n_{e1} - n_{i1})\rvert$<br>$\lvert q_{d0} n_{d1}\rvert >> \lvert n_{d0} q_{d1}\rvert$ | $\lvert q_{d0} n_{d1}\rvert >> \lvert e(n_{e1} - n_{i1})\rvert$<br>$\lvert q_{d0} n_{d1}\rvert \approx \lvert n_{d0} q_{d1}\rvert$ | [10] |
| 9 | Frequency regime | Low | Ultra-low | [9-13] |
| 10 | LFR dispersion in the low-*K* limit | Non-dispersive | NA | Herein |
| 11 | LFR dispersion in the high-*K* limit | Dispersive | NA | Herein |
| 12 | HFR dispersion in the low-*K* limit | NA | Non-dispersive | Herein |
| 13 | HFR dispersion in the high-*K* limit | NA | Dispersive | Herein |
| 14 | Factors affecting phase speed | Plasma parameters in a mixed form | Dust parameters in a pure form | [9-13] |
| 15 | Astro-relevancy | Interstellar media | Compact astroobjects | [9-13] |

Table 5.2: WCL versus SCL

| S. No. | Item | WCL | SCL |
|---|---|---|---|
| 1 | Existencial condition (Coulomb coupling) | $\omega\tau_m << 1$ ($\Gamma_{Cou} << 1$) | $\omega\tau_m >> 1$ ($\Gamma_{Cou} >> 1$) |
| 2 | Viscoelasticity | Irrelevent | Relevent |
| 3 | Dust number density | Low | High |
| 4 | Dust charge | Low | High |
| 5 | Electron number density | Low | High |
| 6 | Ion number density | Low | High |
| 7 | Dust size | Large | Larger |
| 8 | DAW frequency in $\kappa$-case | Low | High |
| 9 | DAW frequency in MB-case | Ultra-high | High |
| 10 | DCW frequency in $\kappa$-case | Ultra-low | Low |
| 11 | DCW frequency in MB-case | Low | Low |
| 12 | $K_c$-shift with $f$ in $\kappa$-case | Less | More |
| 13 | $K_c$-shift with $f$ in MB-case | More | Less |
| 14 | Acoustic fluctuations in $\kappa$-case | NA | HFR |
| 15 | Acoustic fluctuations in MB-case | HFR | HFR |
| 16 | Gravitational fluctuations in $\kappa$-case | Both LFR & HFR | LFR |
| 17 | Gravitational fluctuations in MB-case | LFR | LFR |
| 18 | Instability growth in $\kappa$-case | Less | More |
| 19 | Instability growth in MB-case | More | Less |